analytical chemistry

pubs.acs.org/ac Article

Lab in a Tube: Point-of-Care Detection of *Escherichia coli*

Niloufar Amin,[#] Amadeo Sena Torralba,[#] Ruslan Álvarez-Diduk, Abbas Afkhami, and Arben Merkoçi*

Cite This: *Anal. Chem.* 2020, 92, 4209−4216 Read Online

ACCESS | Metrics & More | Article Recommendations | Supporting Information

ABSTRACT: Significant levels of infectious diseases caused by pathogenic bacteria are nowadays a worldwide matter, carrying considerable public health care challenges and huge economic concerns. Because of the rapid transmission of these biothreat agents and the outbreak of diseases, a rapid detection of pathogens in early stages is crucial, particularly in low-resources settings. To this aim, we developed for the first time a new sensing approach carried out in a single step for *Escherichia coli* O157:H7 detection. The detection principle is based on Förster resonance energy transfer using gold nanoclusters as a signal reporter and gold nanoparticles conjugated with antibodies as a quencher. The sensing platform includes an ultraviolet-light-emitting diode to provide the proper excitation and consists of a microtube containing two pieces of fiber glass; one of them is embedded with label-free gold nanoclusters and the other one with gold nanoparticles conjugated with antibodies. Upon the addition of the sample containing bacteria, the florescence of gold nanoclusters is recovered. The assay was evaluated by the naked eye (on/off) and quantitatively with use of a smartphone camera. The biosensor proved to be highly specific and sensitive, achieving a limit of detection as low as 4.0 cfu mL^{-1}. Additionally, recoveries of 110% and 95% were obtained when the platforms in spiked river and tap water, respectively, were evaluated.

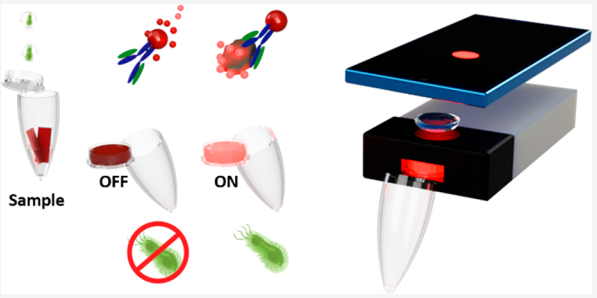

Nowadays, *Escherichia coli* O157:H7 (*E. coli* O157:H7) is one of the major threats to public health care, causing serious infectious diseases mainly through contaminated water and food.[1,2] Because the causative pathogen agent can spread rapidly, it is imperative to achieve a rapid diagnosis. In addition, providing a quick decision in the field to test the safety of water and food will have a great effect on controlling and minimizing mortality rates and financial afflictions.

Traditional methods for the identification and detection of pathogenic bacteria are mainly based on plate cultivation,[3] enzyme-linked immunosorbent assay (ELISA), and polymerase chain reaction (PCR).[4−6] The culturing method requires a long analysis time (ca. days) and special labor operation. PCR and ELISA need significant instruments, manpower, financial resources, and time, all of which already are not suitable for emergency cases, especially in developing countries where medical facilities are unobtainable.[7]

To overcome the aforementioned problems, point-of-care (PoC) diagnostics can be a potential solution for improving global health management.[8] Toward this important goal, different PoC devices for detection of *E. coli* have been implemented, including colorimetric-based lateral flow immunoassay (LFIA)[9−11] and other non-paper-based microfluidic devices based on electrochemical detection,[12] colorimetry,[13,14] fluorimetry,[15] and magneto-fluorimetry.[16] LFIAs are limited by their poor sensitivity, which usually requires signal amplification, whereas other microfluidic systems are relatively expensive and require trained personnel.[17,18] Therefore, there is a lack of suitable PoC devices for detection of *E. coli* for in-field assays.

Our research group has been involved in developing photoluminescence paper-based platforms for detecting *E. coli*.[19,20] The reported strategies are related to the nanoswitch "OFF−ON" methodology using photoluminescent quantum dots conjugated with antibodies. Despite being sensitive and specific, these platforms have some drawbacks, such as multistep procedures and exclusive reader platforms, and especially they are not user-friendly, which reduces the applicability of these biosensors to in-field measurements.

Previous studies have reported the quenching of gold nanoclusters (AuNCs) fluorescence in the presence of gold nanoparticles (AuNPs).[21] This phenomenon occurs because of the complementary overlapping between the surface plasmon resonance absorption wavelength of AuNPs and the fluorescence emission wavelength of AuNCs. Some biosensors have been developed by exploiting this phenomenon, such as the detection of cholesterol[22] and uric acid.[23] In these cases, the detection is carried out through the production of H_2O_2 in an enzymatic reaction; AuNPs seeds start growing, increasing

Received: September 25, 2019
Accepted: February 18, 2020
Published: February 18, 2020

https://dx.doi.org/10.1021/acs.analchem.9b04369
Anal. Chem. 2020, 92, 4209−4216

the absorbance of AuNPs with the consequent decrease in the fluorescence emission of AuNCs. Although this strategy has been exploited for biosensing applications, so far, to the best of our knowledge, none of these nanomaterials have been used together as an immunosensor. Specifically, if we are starting from the OFF state, fluorescence could be recovered if the distance between the donor/acceptor pair becomes big enough.

Certainly, *E. coli* bacteria is big enough to promote this effect. For this purpose, we developed a simple, fast, and cost-effective "lab on a tube" platform for *E. coli* detection. The proposed approach relies on the Förster resonance energy transfer (FRET) mechanism based on gold nanoclusters (AuNCs) as the energy donor and antibody-functionalized AuNPs as the energy acceptor. This enables an ON/OFF fluorescent signal depending on the presence or absence of *E. coli* in the sample. The assay is carried out inside a microtube that contains the reagents embedded in a glass fiber membrane. In this regard, the biosensor can be easily transported and stored up to use. The assay starts by just introducing the sample into the microtube. After 20 min of incubation, the result can be evaluated by the naked eye, during which the presence or absence of fluorescence indicates a yes/no response to the bacteria. Conveniently, it can be evaluated quantitatively by using a three-dimensional (3D) printed device with an ultraviolet-light-emitting diode (UV-LED), a smartphone camera, and an image-analysis app.

EXPERIMENTAL SECTION

Materials and Instruments. All commercial reagents are analytical grade and handled according to the material safety data sheets suggested by the suppliers. Hydrogen tetrachloroaurate(III) dehydrate ($HAuCl_4 \cdot 3H_2O$, 99.9%), trisodium citrate, sodium hydroxide, phosphate buffered saline (PBS) tablet (P4417), and bovine serum albumin (BSA), were purchased from Sigma-Aldrich (Madrid, Spain). Anti-*E. coli* antibody (Ab, ab68451) was obtained from Abcam (Cambridge, UK). *Escherichia coli* O157:H7 (CECT 4783, *E. coli*) and *Salmonella typhimurium* (CECT 722T, *S. typhimurium*) strains were obtained from Sigma-Aldrich (Madrid, Spain). Analytical-grade nitric acid and hydrochloric acid were purchased from Fisher Scientific. The fiber glass membrane (GFCP00080000) was purchased from Millipore. All glassware were washed with aqua regia and rinsed three times with Milli-Q water. Transmission electron microscopy (TEM) images were performed with a FEI Tecnai G2 20 TWIN electron microscope. Fluorescence emission and absorbance spectra were collected on a microplate reader (Molecular Devices). TS-100 Thermo-Shaker (Biosan, Riga, Latvia) was used as the stirrer for functionalization of AuNPs with antibodies.

Synthesis of BSA−AuNCs. BSA−AuNCs were synthesized according to a previous protocol.[24] Briefly, aqueous solutions of $HAuCl_4$ (10 mM, 5 mL) and BSA (50 mg/mL, 5 mL) were mixed and subjected to vigorous stirring at 37 °C. After 2 min, NaOH solution (1.0 M, 0.5 mL) was added to the reaction mixture. The reaction container was sealed and the reaction was allowed to proceed in the dark for 12 h. The solution became deep brown and showed strong red emission under a 365 nm UV lamp, showing the formation of the AuNCs. The prepared AuNCs were purified through a dialysis membrane (molecular weight cut-off: 1 kDa) against Milli-Q water for 1 day to remove unreacted $HAuCl_4$ and sodium hydroxide. Purified AuNCs were kept at 4 °C for further use. The concentration of BSA−AuNCs was estimated at around 20 mg/mL.

Synthesis and Conjugation of AuNPs. The synthesis of AuNPs was performed by following the protocol reported by Bastús and co-workers.[25] In short, the initial AuNPs seeds were prepared by boiling 150 mL of sodium citrate (2.2 mM) in a sealed condenser, followed by the injection of 1 mL of $HAuCl_4$ (25 mM). After 10 min, the color of the solution turned from light yellow to pink and it was cooled, up to 90 °C. Next, 1 mL of sodium citrate (60 mM) was added, and after 2 min, 1 mL of $HAuCl_4$ (25 mM) was sequentially added. The solution was stirred continuously at 90 °C for 30 min and the color of the solution finally became wine-red. The final concentration of the AuNPs solution was 3.1×10^{11} NPs/mL.

The AuNPs were bioconjugated with antibodies against *E. coli* following the procedure previously reported by our group.[26] First, the pH of the AuNPs was adjusted to 8.9 using borate buffer (10 mM). Next, 100 μL of anti-*E. coli* (200 μg/mL) were incubated with 1.5 mL of AuNPs for 24 h at 350 rpm and 4 °C. Then 100 μL of BSA solution in Milli-Q water (final concentration 1% (w/w)) was added to the conjugated AuNPs followed by incubation for 1 h under the previous conditions. The excess of antibodies and BSA were removed by centrifuging the solution at 14 000 rpm and 4 °C for 30 min, followed by resuspension with 200 μL of Milli-Q water. Finally, the conjugated AuNPs where stored at 4 °C for further use.

Platform Fabrication. The glass fiber membranes were cut into 15 cm × 8 mm strips. Eight hundred microliters of the conjugated AuNPs and AuNCs where drop-casted on separate glass fiber strips and dried in a vacuum chamber for 2.5 h. Finally, they were cut in circles (diameter ≈0.6 cm) with use of a hole puncher, and then they were introduced into the microtubes.

Bacteria Preparation. Stock solution (1010 *E. coli*/mL) of bacteria was prepared by dissolving 10 mg of *E. coli* in 1 mL of filtered Milli-Q water followed by shaking with a vortex. To determine the concentration of the prepared stock solution, we measured the optical density at 600 nm (OD_{600}) using a spectrophotometer that was corroborated with Agilent geometry software (https://www.chem.agilent.com/store/biocalculators/calcODBacterial.jsp). Standard serial solutions of *E. coli* (0−10^8 cfu/mL) were prepared by diluting the suspension stock solution (1010 cfu/mL ≈ 1010 *E. coli*/mL) in PBS.

Assay Performance. Serial dilutions of *E. coli* (0−10^8 cfu/mL) were prepared in PBS, 200 μL was drop-casted into the microtube and incubated for 20 min at room temperature. The assay was evaluated with a spectrophotometer by transferring the solution into a microplate. The fluorescence intensity was measured at 665 nm (Ex. 365 nm) for each dilution of *E. coli* and normalized with the blank ($F - F_0$), where F and F_0 corresponded to the sample with and without *E. coli*, respectively. For a point-of-care application, the assay was evaluated by taking a picture using a smartphone camera and analyzing the picture with ImageJ software (National Institutes of Health, Maryland, USA) following the protocol already reported by our group.[27] All the experiments were replicated three times.

RESULTS AND DISCUSSION

Assay Principle. The assay was performed in a polypropylene microtube, which was used as a reservoir and detection platform. First, the fluorescent AuNCs were

https://dx.doi.org/10.1021/acs.analchem.9b04369
Anal. Chem. 2020, 92, 4209−4216

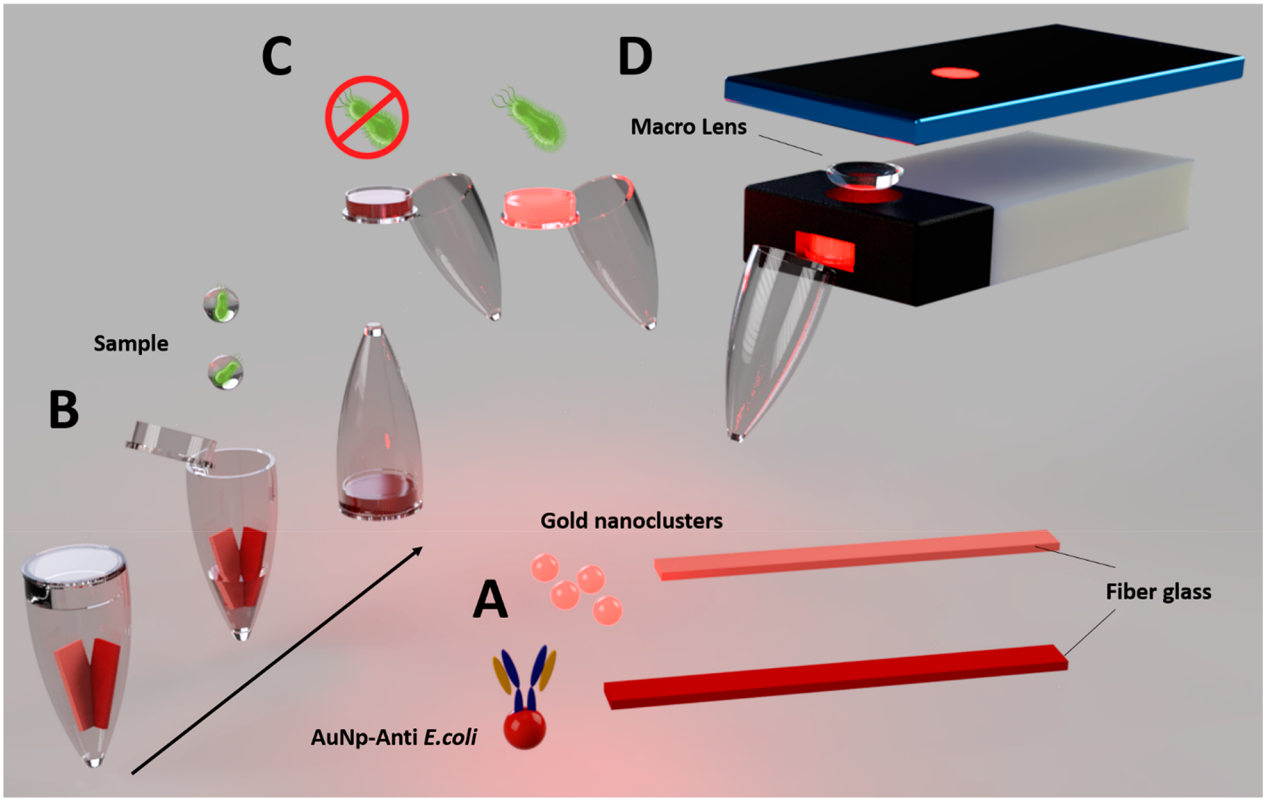

Figure 1. Schematic representation of the biosensing platform. (A) Two fiber glass strips embedded with AuNCs and AuNPs conjugated with anti-*E. coli* antibody, respectively. (B) Operation principle; sample is added directly to the microtube containing the two strips. (C) Naked eye evaluation of the ON/OFF switch mechanism. (D) Smartphone-based device for quantitative evaluation of the *E. coli* concentration.

synthesized, purified, and drop-casted onto a fiberglass membrane. The fiber glass was then dried using a vacuum desiccator and cut into circular pieces (⌀ 0.6 cm) using a hole puncher. The pieces were introduced into the microtube and stored until the assay was run. The same procedure was done for the AuNPs, which were previously conjugated with antibodies against *E. coli* O157:H7 following the procedure reported in the Experimental Section (Figure 1A). In this way, the microtube stocked both conjugate pads, one containing the sensing PL probe (AuNCs) and the other containing the quencher label (AuNPs). The fiber glass was used as a porous material with high absorption and release capacity of solutions, appropriate long-term storage of samples, high stability, and good flexibility.[28,29] For evaluation of the presence of *E. coli* in a real environment, the assay starts by introducing the sample solution into the microtube followed by a 20 min incubation step (Figure 1B). The sample solution enables the rehydration of the conjugate pad and the eventual release of the stored nanomaterials to the solution. The biosensing mechanism is based on Förster resonance energy transfer (FRET), the AuNPs and AuNCs being the energy acceptors and donors, respectively. In this regard, the AuNPs were able to quench the fluorescence emission of the AuNCs when they were close together. This is known as the "turn-off" mode, which is linked to the absence of *E. coli* in the sample. Conversely, in the presence of *E. coli*, the antibody-functionalized AuNPs attached to the surface of the bacteria, avoiding the approach of the AuNCs. In this way, due to the fact that the FRET mechanism is possible up to 30 nm and the *E. coli* were 1 μm in size,[30] the fluorescence signal was restored, switching to a "turn-on" mode (Figure 1C). Notice the specificity of the assay. In this regard, AuNCs were mixed with AuNPs with and without bacteria. As observed in Figure S1 (Supporting Information), there is no recovery in the fluorescence of AuNCs when AuNPs are not conjugated with antibodies.

Finally, a quantitative outcome was obtained using a smartphone camera. Nowadays, almost any smartphone has a good quality complementary metal−oxide−semiconductor sensor and the possibility to fix the picture parameters such as shutter speed, ISO, and focus, obtaining reproducible and accurate images. In this regard, a 3D-printed device was developed to introduce the microtube using the cap as the sample holder. The device contains a 365 nm UV-LED to excite the AuNCs and a macro lens to adjust the focal length of the camera to the minimum possible (Figure 1D). The pictures were analyzed using ImageJ app (smartphone version) to transform the brightness levels into a numerical value, which allows quantification. Because most people across the world have a smartphone as a common device used in their day-to-day lives, this proof of concept makes a highly promising device for point-of-care assay and field applications without the need for a conventional bulky analyzer such as a fluorimeter.

Characterization of AuNCs and Conjugated AuNPs. The synthesized AuNCs were characterized by transmission electron microscopy (TEM). As observed in Figure 2A, they have a uniform morphology and a narrow size distribution with an average diameter of about 1.0 nm. Furthermore, a fluorescence emission peak appeared at 665 nm when excited at 365 nm and a strong red emission under UV light (Figure 2B). The synthesized AuNPs were also characterized with TEM, as shown in Figure 2C,D. AuNPs have a spherical and uniform size of around 40 nm. Besides, its conjugation to

https://dx.doi.org/10.1021/acs.analchem.9b04369
Anal. Chem. 2020, 92, 4209−4216

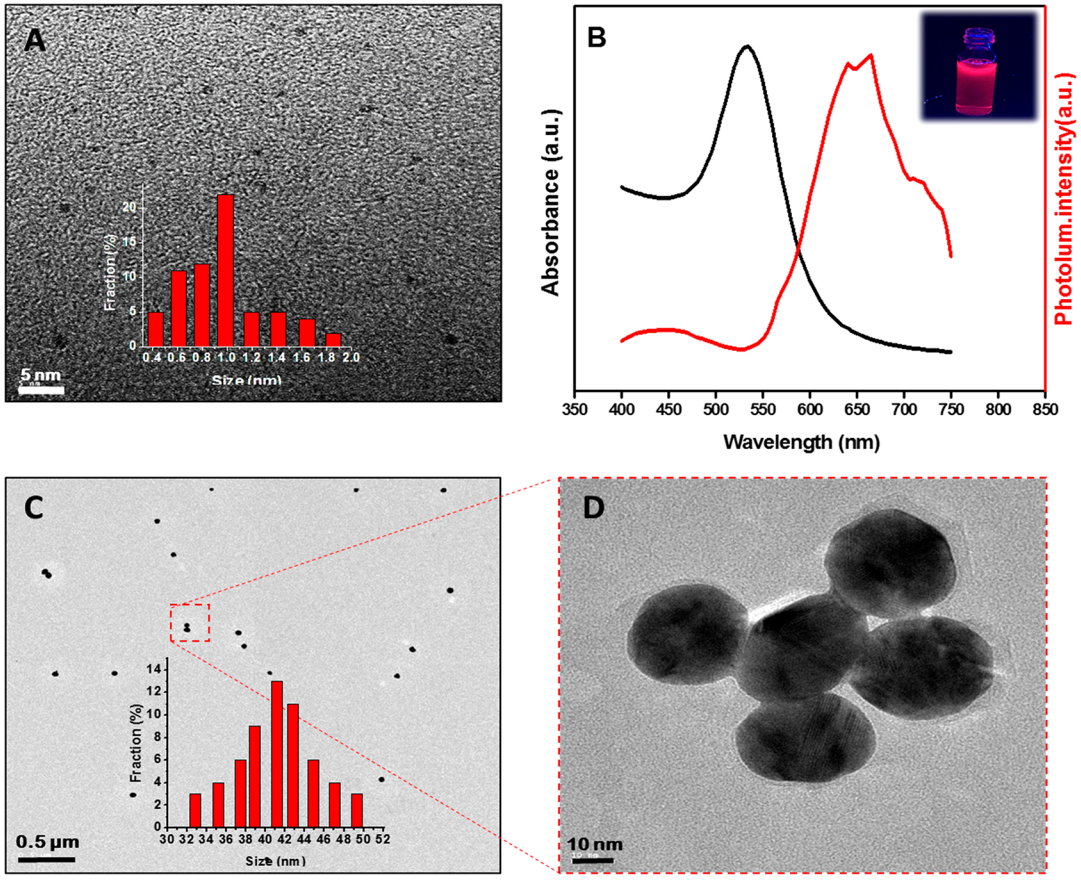

Figure 2. (A) TEM image of BSA−AuNCs. Inset: Size distribution histogram of the as-prepared AuNCs. (B) Fluorescence spectra of BSA−AuNCs (red line) and absorption spectrum of conjugated AuNPs with anti-*E. coli* (black line). Inset: Digital photograph of AuNCs under UV light. (C) TEM image of citrate-stabilized AuNPs. Inset: Graph corresponds to the size distribution diagram. (D) High magnification of as-prepared AuNPs.

antibodies against *E. coli* was corroborated by the presence of a red shift from 525 to 535 nm in the UV−vis spectrum, indicating modification of the AuNPs surface (Figure S2).[31] Finally, for achieving FRET, the absorbance spectrum of the energy acceptor must be overlapped with the emission spectrum of the donor probe. This phenomenon can be observed in Figure 2B, where the emission spectrum of the AuNCs was clearly overlapped with the absorbance spectrum of the conjugated AuNPs.

Assay Optimization. The highest concentration with the higher fluorescence emission of AuNCs was tested to evaluate the size dependence on the quenching efficiency of AuNPs. The bigger the size of the nanoparticles, the higher the red shift in the wavelength, causing more overlap with the emission of AuNCs.[21] Among the tested sizes, 40 nm was selected as the most suitable for the assay (Figure S3). Besides bigger nanoparticles (>40 nm) producing more quenching, the antibodies conjugation protocols are fully optimized for 40 nm. Moreover, if bigger nanoparticles are used, the required amount of antibodies to cover the surface will be higher, causing a more expensive device. For evaluation of how the AuNPs concentration affects the quenching of AuNCs, the stock solution (3.1×10^{11} NPs/mL) of the AuNPs was concentrated (by centrifugation) and diluted. It can be observed in Figure 3A that indeed higher concentrations of AuNPs produce more quenching on the light emission of AuNCs. Nevertheless, we have selected 1.16×10^{12} NPs/mL as a compromise between efficiency and affordability because there is no noteworthy quenching at higher concentrations.

Furthermore, the antibody concentration on the AuNPs was also optimized as it dramatically affects the sensitivity and the cost-effectiveness of the platform (using less antibody can considerably reduce the development cost of the biosensor). This was done by performing the well-stablished gold aggregation test (GAT),[32] which determines the maximum concentration of antibody required to cover the AuNPs surface. On the basis of the results shown in Figure 3B, we concluded that 175 μg/mL of anti-*E. coli* were enough to cover the surface of the AuNPs; however, we rounded it up to 200 μg/mL in the subsequent assays.

The required concentration of AuNCs to achieve an effective FRET and recovery was another parameter to be optimized. In this context (AuNPs at a fixed concentration of 1.16×10^{12} NPs/mL) the fluorescence recovery in the presence of *E. coli* was evaluated using different AuNCs concentrations (from 0.5 to 8.0 mg/mL). As expected, an excess of AuNCs brought signal saturation, whereas a low concentration of AuNCs led to negligible fluorescence intensity (Figure 3C). Therefore, the fluorescence enhancement efficiency ($F - F_0$) was employed as a criterion to evaluate the best signal, where F and F_0 correspond to the intensities of fluorescence of the AuNCs/AuNPs system in the presence and absence of *E. coli*, respectively. Hereby, 6.0 mg/mL was determined to be the optimal concentration of AuNCs.

https://dx.doi.org/10.1021/acs.analchem.9b04369
Anal. Chem. 2020, 92, 4209−4216

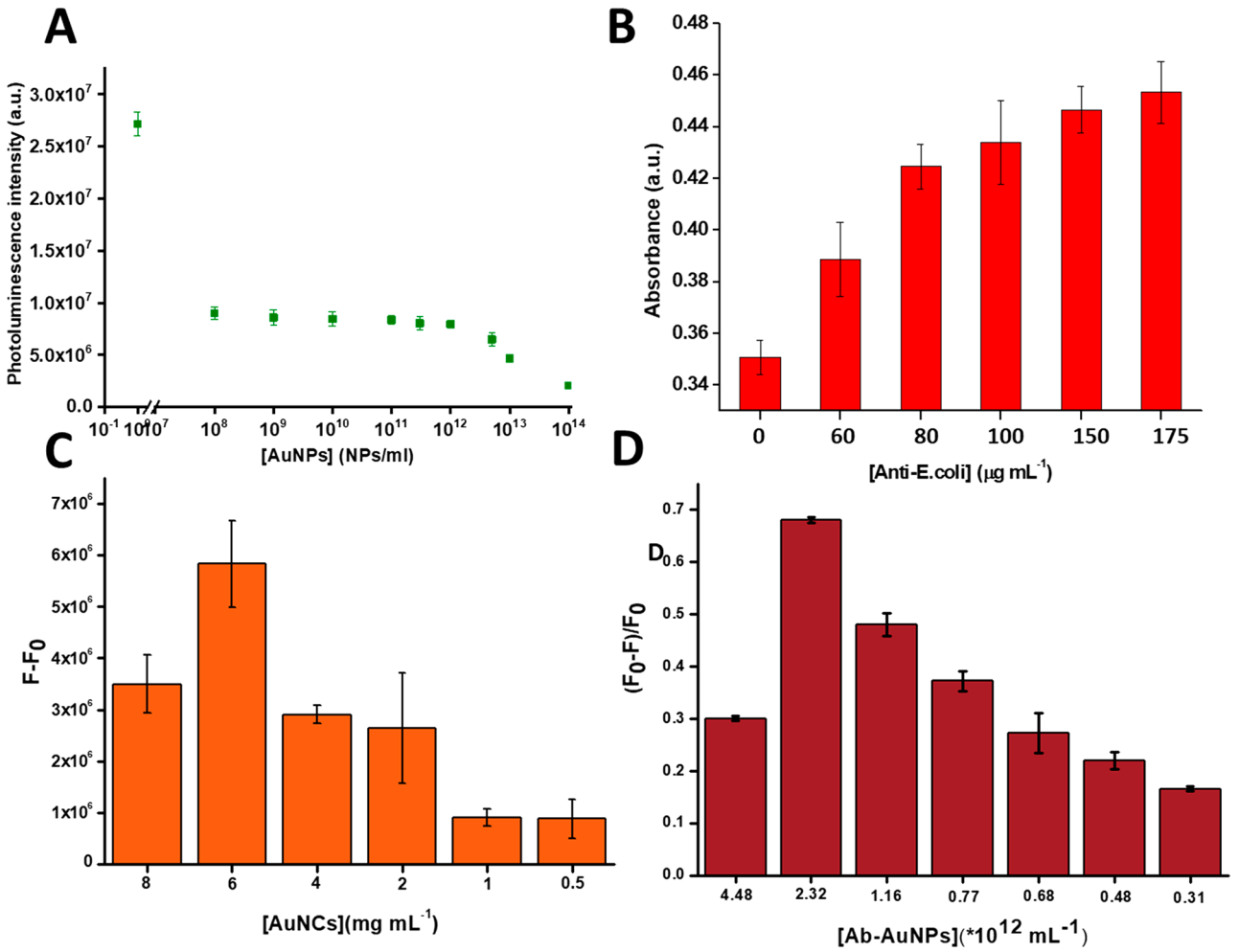

Figure 3. Optimization of experimental conditions. (A) Preoptimization of the quenching efficiency due to AuNPs concentration. (B) Effect of the concentration of the immobilized antibody on the surface of AuNPs (GAT) at NaCl 1% and 0.58 × 10^{12}/mL AuNPs in various concentrations of antibody. (C) Effect of the concentration of AuNCs as a fluorophore agent on fluorescence recovery efficiency ($F - F_0$), where F and F_0 correspond to the fluorescence intensities of the AuNCs/AuNPs system in the presence and absence of *E. coli*, respectively, at 10^5 cfu/mL *E. coli*. (D) Effect of the concentration of anti-*E. coli*-labeled AuNPs on quenching efficiency $(F_0 - F)/F_0$, where F and F_0 correspond to the fluorescence intensities of AuNCs in the presence and absence of Ab-AuNPs, respectively. The concentration of AuNCs was 6.0 mg/mL.

Although AuNPs concentration was previously optimized (preoptimization strategy), those nanoparticles were not conjugated with anti-*E. coli* antibodies. It is important to double check the concentration of conjugated AuNPs required to achieve an effective FRET, taking into consideration the previously optimized AuNCs concentration. In this regard, conjugated AuNPs ranging from 0.31 to 4.46 (×10^{12} NPs/mL) were evaluated. As observed in Figure 3D, 2.32 (×10^{12} AuNPs/mL) allowed a 68% quenching efficiency, whereas higher and lower concentrations ended up with signal saturation and low quenching, respectively. It is also essential to optimize this parameter for fluorescence restoration efficiency (Figure S4). Therefore, this was the concentration of conjugated AuNPs selected for the next experiments.

Finally, to better understand the response rate of our platform to *E. coli* detection, we performed a comprehensive kinetics study (Figure S5), showing that the fluorescence signal increased exponentially and reached equilibrium after 20 min. This reveals the assay time required before performing the final evaluation.

Smartphone-Based Detection of *E. coli*. The developed platform was first evaluated under optimal conditions by spiking known concentrations of *E. coli* (from 0 to 10^7 cfu/mL) in PBS buffer (10 mM, pH 7.4) and using a spectrophotometer. As observed in Figure 4A, the fluorescence signal gradually increases with a higher concentration of *E. coli*, with a good correlation (exponential behavior log[*E. coli*]) from 0 to 10^5 cfu/mL (Figure 4B), F and F_0 being the fluorescence intensities at 665 nm in the presence and absence of *E. coli*, respectively. The limit of detection (LOD) was calculated as low as 1.37 cfu/mL based on 3 times "s/m" ratio, where "s" is the standard deviation of the blank fluorescence signal (three replicates) and "m" is the slope of the related calibration curve. Furthermore, the assay was evaluated with a smartphone camera to get as close as possible to point-of-care conditions. In this context, a Samsung Galaxy S7 smartphone was used to take a picture of the microtubes after running the assay (20 min incubation). The microtube cap was irradiated under a UV-LED (Ex. 365 nm) and the smartphone was attached to a holder; the pictures were always taken in the same conditions: At ISO 100 and shooter speed 1/60 s. As illustrated in Figure 4C, the sample containing 0 cfu/mL of *E. coli*, defined as the blank sample, is characterized by low brightness levels because of the "turn-off" FRET effect.

https://dx.doi.org/10.1021/acs.analchem.9b04369
Anal. Chem. 2020, 92, 4209−4216

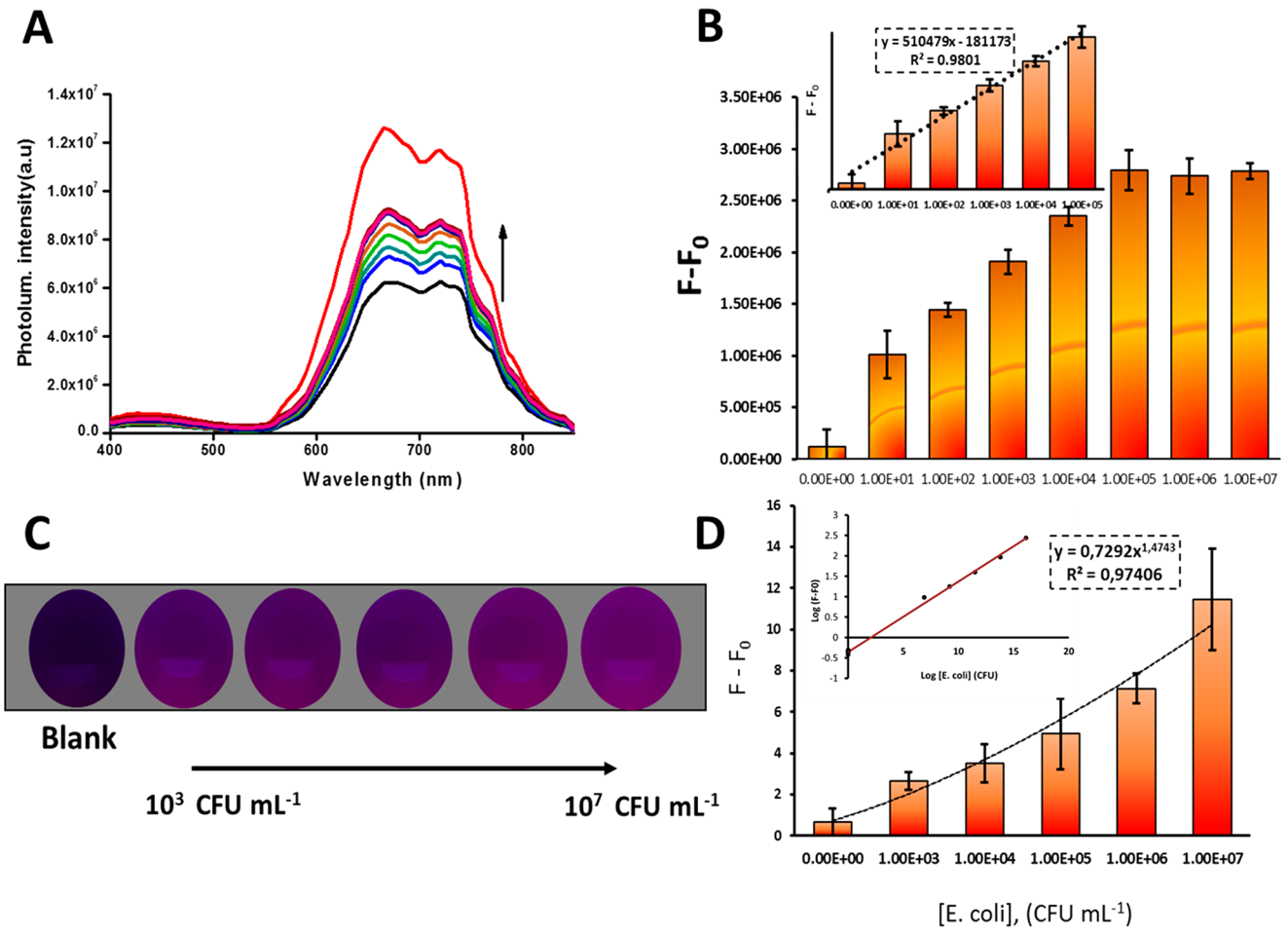

Figure 4. Quantification of *E. coli* O157:H7 using a developed biosensor. (A) Fluorescence spectrum of AuNCs/Ab-AuNPs upon addition of different concentrations of *E. coli* from 0 to 10^7 cfu/mL. (B) Calibration curve of the assay using a fluorimeter. (F and F_0 correspond to the fluorescence intensities of the AuNCs/AuNPs system in the presence and absence of *E. coli*, respectively). (C) Typical images of the AuNCs/Ab-AuNPs system in the presence of various concentrations of *E. coli* in the range of 0–10^7 cfu/mL (0, 10^3, 10^4, 10^5, and 10^6 cfu/mL from left to right) captured using a smartphone camera under 365 nm UV light irradiation. (D) Calibration curve resulting from processing images in the smartphone. Error bars represent the standard deviation (n = 3). Inset: linear behavior of a power function.

However, with the increase of *E. coli* concentration, there was a gradual increase in fluorescence ("turn-on" mode). To obtain a numerical value, we analyzed the pictures with ImageJ software, in which the fluorescence intensity is transformed into a value from 0 to 255 (where 0 is dark and 255 is maximum brightness). The fluorescence intensity values were normalized with the signal corresponding to the absence of *E. coli* (F_0). The calibration curve is observed in Figure 4D, which shows a power fluorescence increase. It is worth noticing a change in the mathematical function in light of the results obtained with the fluorimeter and the smartphone. When the values according to the function obtained with the fluorometer (log[*E. coli*]) are graphed, exponential behavior can be seen, which means that the results obtained with the smartphone follow a power function from 0 to 10^7 cfu/mL with a LOD of 4.0 cfu/mL (Figure 4D inset).

The developed biosensor performance of *E. coli* detection was compared to some of the reported point-of-care sensors and summarized in Table S1.

Real Samples Evaluation. To further test the practicability of the biosensor, we conducted the assay by spiking known concentrations of *E. coli* (10^2 and 10^5 cfu) to tap water and river water samples collected from the river Ter (Vic, Spain). The samples were evaluated following the procedure previously reported and the recoveries were calculated by comparing the results obtained in real samples (i) with the ones obtained in PBS (ii), using the following equation:

$$\text{recovery (\%)} = 100 \times (F - F_0)^{i} / (F - F_0)^{ii}$$

The results are summarized in Table 1. The obtained recoveries prove that there is no drastic interference when evaluating samples with a complex matrix; thus, the developed

Table 1. Detection of *E. coli* Bacteria Spiked in Water Samples (n = 3)

sample	spiked *E. coli* (cfu/mL)	$F - F_0$# in standard buffer	$F - F_0$* in real samples	recovery[a] (%)
river water	10^2	1440843	1503611	103.70
	10^5	2791463	2648975	105.37
tap water	10^2	1440843	1400975	97.23
	10^5	2783852	2740975	98.45

[a]Recovery (%) = 100 × ($F - F_0$*/$F - F_0$#).

https://dx.doi.org/10.1021/acs.analchem.9b04369
Anal. Chem. 2020, 92, 4209–4216

platform can be applied for the detection of *E. coli* in real samples at the point of care.

Determination of the Assays Specificity. The specificity of the biosensor toward *E. coli* was assessed by evaluation samples containing *E. coli* and *S. typhimurium*, which is a similar family pathogen. Dilutions of *E. coli*, *S. typhimurium*, and a mixture of both bacteria where spiked in PBS. The assay was carried out following the previous procedure. As shown in Figure 5, the normalized fluorescence (FL) intensity increased

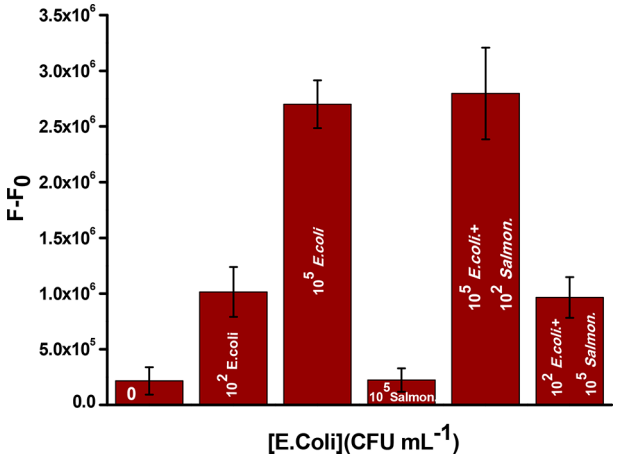

Figure 5. Specificity of the developed fluorescence biosensor toward *E. coli* in the presence of *S. typhimurium* as interfering bacteria. The error bars are the standard deviation of the three measurements.

with higher concentrations of *E. coli* (from 0 to 10^5 cfu/mL). Conversely, the normalized FL intensity obtained for a sample with 10^5 cfu/mL of *S. typhimurium* was similar to the one obtained for 0 cfu of *E. coli*. This result proves that the developed biosensor was specific only for *E. coli* because of the AuNPs functionalization with highly specific antibodies against *E. coli* O157:H7. This was further corroborated by evaluating solutions containing a mixture of 10^5 cfu/mL *S. typhimurium* + 10^2 cfu/mL *E. coli* and 10^5 cfu/mL *E. coli* + 10^2 cfu/mL *S. typhimurium*. In the first case, the obtained signal was similar to the blank (0 cfu/mL *E. coli*) and in the second case the signal was similar to the one obtained for 10^5 cfu/mL *E. coli*. Therefore, the results confirmed that the platform has a high specificity response, and when applied in real samples, the achieved signal could be linked only to *E. coli* detection.

CONCLUSIONS

The proposed all-in-one device combines the outstanding advantage of both the glass fiber membrane as a cost-effective substrate with high loading capacity and the microtube platform as a simple and portable setup. Moreover, the detection method applied in the developed biosensor is fast (20 min) and does not require washing steps. It has proved to be highly sensitive and specific for detection of *E. coli*, although its application can be extended to other large analytes. Finally, the possibility to do smartphone-based detection empowers the developed biosensor as unique PoC tests with real applicability in resources-limited settings.

ASSOCIATED CONTENT

Supporting Information

The Supporting Information is available free of charge at https://pubs.acs.org/doi/10.1021/acs.analchem.9b04369.

AuNCs quenching with AuNPs with and without bacteria in absence of specific receptors; UV−vis spectra of AuNPs and Ab-AuNPs; effect of concentration of Ab-AuNPs on the photoluminescence restoration; kinetic behavior studies of AuNCs/Ab-AuNPs in the presence of *E. coli*; comparison of the experimental and analytical performance of the present method with other point-of-care platforms for *E. coli* detection (PDF)

AUTHOR INFORMATION

Corresponding Author

Arben Merkoçi − *Nanobioelectronics & Biosensors Group, Catalan Institute of Nanoscience and Nanotechnology (ICN2), CSIC and BIST, Campus UAB, Bellaterra, Barcelona 08193, Spain; ICREA, Institució Catalana de Recerca i Estudis Avançats, Barcelona 08010, Spain;* orcid.org/0000-0003-2486-8085; Email: arben.merkoci@icn2.cat

Authors

Niloufar Amin − *Nanobioelectronics & Biosensors Group, Catalan Institute of Nanoscience and Nanotechnology (ICN2), CSIC and BIST, Campus UAB, Bellaterra, Barcelona 08193, Spain; Faculty of Chemistry, Bu-Ali Sina University, Hamedan, Iran; Food and Drug Laboratory Research Center, Food and Drug Organization, MOH&ME, Tehran, Iran;* orcid.org/0000-0001-9743-0418

Amadeo Sena Torralba − *Nanobioelectronics & Biosensors Group, Catalan Institute of Nanoscience and Nanotechnology (ICN2), CSIC and BIST, Campus UAB, Bellaterra, Barcelona 08193, Spain*

Ruslan Álvarez-Diduk − *Nanobioelectronics & Biosensors Group, Catalan Institute of Nanoscience and Nanotechnology (ICN2), CSIC and BIST, Campus UAB, Bellaterra, Barcelona 08193, Spain;* orcid.org/0000-0002-9876-1574

Abbas Afkhami − *Faculty of Chemistry, Bu-Ali Sina University, Hamedan, Iran;* orcid.org/0000-0002-3559-2080

Complete contact information is available at: https://pubs.acs.org/10.1021/acs.analchem.9b04369

Author Contributions

#N.A. and A.S.T. contributed equally to this work.

Notes

The authors declare no competing financial interest.

ACKNOWLEDGMENTS

The ICN2 is funded by the CERCA Programme/Generalitat de Catalunya. The ICN2 is supported by the Severo Ochoa program of the Spanish Ministry of Economy, Industry and Competitiveness (MINECO, gGrant No. SEV-2017-0706). Financial support was obtained under the MINECO Project MAT2017-87202-P. N.A. acknowledges the Food and Drug Laboratory Research Center, Food and Drug Organization of Iran, and Ministry of Science, Research and Technology of Iran for scholarships during this research time. A.S.T. acknowledges Universitat Autònoma de Barcelona for the possibility of carrying out this work inside the framework of its PhD Programme in Biotechnology.

REFERENCES

(1) Painter, J. A.; Hoekstra, R. M.; Ayers, T.; Tauxe, R. V.; Braden, C. R.; Angulo, F. J.; Griffin, P. M. *Emerging Infect. Dis.* **2013**, *19* (3), 407.

(2) Scallan, E.; Griffin, P. M.; Angulo, F. J.; Tauxe, R. V.; Hoekstra, R. M. *Emerging Infect. Dis.* **2011**, *17* (1), 16.
(3) Opota, O.; Croxatto, A.; Prod'hom, G.; Greub, G. *Clin. Microbiol. Infect.* **2015**, *21* (4), 313−322.
(4) Souza, R. B.; Trevisol, D. J.; Schuelter-Trevisol, F. *Braz. J. Infect. Dis.* **2015**, *19* (3), 319−323.
(5) Zourob, M.; Elwary, S.; Turner, A. P. *Principles of bacterial detection: biosensors, recognition receptors and microsystems*; Springer Science & Business Media: 2008.
(6) Zhao, Z.; Yan, R.; Yi, X.; Li, J.; Rao, J.; Guo, Z.; Yang, Y.; Li, W.; Li, Y.-Q.; Chen, C. *ACS Nano* **2017**, *11* (5), 4428−4438.
(7) Russo, L.; Leva Bueno, J.; Bergua, J. F.; Costantini, M.; Giannetto, M.; Puntes, V.; de la Escosura-Muñiz, A.; Merkoçi, A. *ACS Omega* **2018**, *3* (12), 18849−18856.
(8) Yetisen, A. K.; Akram, M. S.; Lowe, C. R. *Lab Chip* **2013**, *13* (12), 2210−2251.
(9) Huang, H.; Zhao, G.; Dou, W. *Biosens. Bioelectron.* **2018**, *107*, 266−271.
(10) Luo, K.; Hu, L.; Guo, Q.; Wu, C.; Wu, S.; Liu, D.; Xiong, Y.; Lai, W. *J. Dairy Sci.* **2017**, *100* (7), 5176−5187.
(11) Wu, W.; Zhao, S.; Mao, Y.; Fang, Z.; Lu, X.; Zeng, L. *Anal. Chim. Acta* **2015**, *861*, 62−68.
(12) Li, Y.; Xiong, Y.; Fang, L.; Jiang, L.; Huang, H.; Deng, J.; Liang, W.; Zheng, J. *Theranostics* **2017**, *7* (4), 935.
(13) Chen, J.; Alcaine, S. D.; Jackson, A. A.; Rotello, V. M.; Nugen, S. R. *ACS Sens* **2017**, *2* (4), 484−489.
(14) Lagally, E.; Scherer, J.; Blazej, R.; Toriello, N.; Diep, B.; Ramchandani, M.; Sensabaugh, G.; Riley, L.; Mathies, R. *Anal. Chem.* **2004**, *76* (11), 3162−3170.
(15) Sugino, H.; Ozaki, K.; Shirasaki, Y.; Arakawa, T.; Shoji, S.; Funatsu, T. *Lab Chip* **2009**, *9* (9), 1254−1260.
(16) Banerjee, T.; Sulthana, S.; Shelby, T.; Heckert, B.; Jewell, J.; Woody, K.; Karimnia, V.; McAfee, J.; Santra, S. *ACS Infect. Dis.* **2016**, *2* (10), 667−673.
(17) Zarei, M. *Biosens. Bioelectron.* **2018**, *106*, 193−203.
(18) Nasseri, B.; Soleimani, N.; Rabiee, N.; Kalbasi, A.; Karimi, M.; Hamblin, M. R. *Biosens. Bioelectron.* **2018**, *117*, 112−128.
(19) Cheeveewattanagul, N.; Morales-Narváez, E.; Hassan, A. R. H.; Bergua, J. F.; Surareungchai, W.; Somasundrum, M.; Merkoçi, A. *Adv. Funct. Mater.* **2017**, *27* (38), 1702741.
(20) Morales-Narváez, E.; Naghdi, T.; Zor, E.; Merkoçi, A. *Anal. Chem.* **2015**, *87* (16), 8573−8577.
(21) Qin, H.; Ma, D.; Du, J. *Spectrochim. Acta, Part A* **2018**, *189*, 161−166.
(22) Chang, H.-C.; Ho, J.-a. A. *Anal. Chem.* **2015**, *87* (20), 10362−10367.
(23) Liu, Y.; Li, H.; Guo, B.; Wei, L.; Chen, B.; Zhang, Y. *Biosens. Bioelectron.* **2017**, *91*, 734−740.
(24) Xie, J.; Zheng, Y.; Ying, J. Y. *J. Am. Chem. Soc.* **2009**, *131* (3), 888−889.
(25) Bastús, N. G.; Comenge, J.; Puntes, V. *Langmuir* **2011**, *27* (17), 11098−11105.
(26) Haiss, W.; Thanh, N. T.; Aveyard, J.; Fernig, D. G. *Anal. Chem.* **2007**, *79* (11), 4215−4221.
(27) Álvarez-Diduk, R.; Orozco, J.; Merkoçi, A. *Sci. Rep.* **2017**, *7* (1), 976.
(28) Oyama, Y.; Osaki, T.; Kamiya, K.; Kawano, R.; Honjoh, T.; Shibata, H.; Ide, T.; Takeuchi, S. *Lab Chip* **2012**, *12* (24), 5155−5159.
(29) O'Farrell, B. Evolution in lateral flow−based immunoassay systems. In *Lateral flow immunoassay*; Springer: 2009; pp 1−33.
(30) Morales-Narváez, E.; Hassan, A. R.; Merkoçi, A. *Angew. Chem., Int. Ed.* **2013**, *52* (51), 13779−13783.
(31) Chen, W.; Cao, F.; Zheng, W.; Tian, Y.; Xianyu, Y.; Xu, P.; Zhang, W.; Wang, Z.; Deng, K.; Jiang, X. *Nanoscale* **2015**, *7* (5), 2042−2049.
(32) Ambrosi, A.; Castañeda, M. T.; Killard, A. J.; Smyth, M. R.; Alegret, S.; Merkoçi, A. *Anal. Chem.* **2007**, *79* (14), 5232−5240.

https://dx.doi.org/10.1021/acs.analchem.9b04369
Anal. Chem. 2020, 92, 4209−4216